Project Title:

Theoretical study of interaction between tunneling electrons and individual molecules at surfaces

Name:Yousoo Kim, Kuniyuki Miwa, Emiko Kazuma, Emi Minamitani, Hiroshi Imada, Jaehoon Jung, Miyabi Imai
Laboratory at RIKEN:Surface and Interface Science Laboratory

1. Background and purpose of the project, relationship of the project with other projects.

During the past decade, computer simulations based on a quantum mechanics have developed an increasingly important impact not only on solid-state physics and chemistry but also on materials science. In material science, the surface chemistry is fundamentally essential in many areas, such as molecular electronics, heterogeneous catalyst, storage materials, sensors, and so forth. The adsorption of molecules onto a surface is a necessary prerequisite to any surface-mediated chemical process. Understanding the bonding nature between the molecule and the surface on the basis of the electronic structure is therefore one of the most important issues in this field. The computational methods like density functional theory (DFT) have played a prominent role to elucidate the interaction between the molecule and the surface. In addition, the computational method can be useful to study the details of energy transport and conversion among photon and electrons mediated with adsorbate at solid surfaces in the nanoscale regime.

From the theoretical investigation of the adsorbed molecule on surface in combination with scanning tunneling microscopy and spectroscopy (STM/STS) experiment, we could expect the following research goals; 1) the deep understanding of the chemical/physical properties of an adsorbate on the surface not only in ground state but also in excited state, 2) the fine control of the chemistry on the surface.

2. Specific usage status of the system and calculation method

We have been studying the molecular adsorption on the well-defined metal surface using computational method in combination with experimental method. In our studies, first-principles simulations have been carried out using the Vienna Ab-initio Simulation Package (VASP) code in the density functional level of theory. The pure DFT methods have been mostly used and the inner electrons are replaced by projector augmented wave pseudopotentials (PAW). The climbing image nudged elastic band method (CI-NEB) was used to determine the transition states that were confirmed by imaginary frequency modes. In most of cases, STM image simulations were performed using Tersoff-Hamann approach. The computational results have been compared with the available experimental result obtained from STM in our group. For the gas phase molecules, the Gaussian09 program with atomic-orbital basis set was also effectively utilized to obtain stable geometries and corresponding electronic structures.

We also have been studying the many-body phenomena in molecular adsorption system, in particular the Kondo effect. The characteristic electronic state resulting from the Kondo effect, so-called Kondo singlet state appears as a sharp peak structure (Kondo peak) at the Fermi level (E_F) in STS. In order to simulate the Kondo peak, we build numerical renormalization group (NRG) code and the STS simulation code based on the Keldysh Green's function method.

3. Results

(1) Functionalization of graphene grown on metal substrate with atomic oxygen: graphene enolate

Functionalization of graphene has attracted great scientific interest, not only in controlling the physical properties of graphene, e.g., opening band gap to achieve semiconducting nature, but also in improving chemical adaptability to integrate graphene as a building block into a variety of functional devices. Due to the great simplicity of the atomic species, atomic functionalization on the basal plane of graphene with covalent bonds is considered a promising way to maximize the usefulness of graphene. In particular, atomic oxidation allows compositional expandability through additional chemical reactions. At the limit of low coverage, whereas hydrogen or fluorine makes a single covalent bond with a C atom, i.e., "on-top configuration", on the basal plane of a graphene sheet, the attachment of atomic oxygen to graphene results in graphene epoxide, i.e., "bridge configuration", in which an O atom covalently interacts with two adjacent C atoms, which has been proved by a number of experiment and theoretical calculations. However, other possibilities besides an epoxy group on the basal plane of graphene have been excluded, narrowing the choices of a chemical route not only for further functionalization but also for the development of graphene-based catalysts. In this study, we first suggest that atomic oxidation of graphene grown on a metal substrate results in the formation of graphene enolate, i.e., negatively charged oxygen adsorbed at the on-top position on its basal plane, which is strikingly different from the formation of epoxy groups on free-standing graphene and on graphite. Whereas the enolate is the transition state between two neighboring epoxides on free-standing graphene and on graphite, we revealed that the enolate group formed on epitaxial graphene on a metal substrate exists as a local minimum, and further becomes more stable than the epoxide.

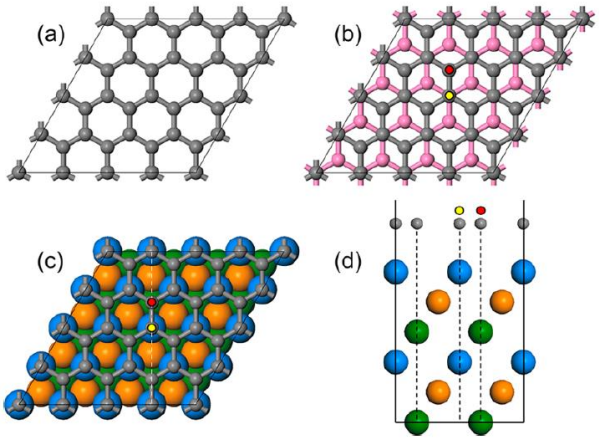

Figure 1. Simulated (4×4) supercell structures for (a) free-standing graphene, (b) graphite, and (c,d) graphene grown on metal substrate, Cu(111). The cross-section corresponding to (d) is indicated by a dashed white line in (c). The vertical positions of C atoms with respect to metal substrate are indicated by dashed black lines in (d). Red and yellow dots indicate two different on-top configurations, OT1 and OT2, respectively, for atomic oxygen adsorbate.

To examine atomic oxidation of a graphene sheet grown on a metal substrate, we performed periodic DFT calculations, at the level of local density approximation (LDA) implemented in VASP code, for graphenes epitaxially grown on Cu(111), i.e., Gr/Cu(111). Computational results for Gr/Cu(111) were also compared with those for free-standing graphene and graphite. We assumed (1×1) epitaxial graphene on the Cu(111) substrate for simplicity, which leads to only 1.9% lengthening of the lattice constant of graphene at the level of LDA. Figure 1 shows the (4×4) supercell structures employed in this study. Whereas free-standing graphene has only one type of on-top site for atomic oxidation on its basal plane (Fig. 1a), there are two different on-top configurations (OT1 and OT2, red and yellow dots, respectively), corresponding to the formation of graphene enolate, on graphite and Gr/Cu(111) (Figs. 1b and 1c). The C atoms (β) adjacent to the oxidized C atom (α) locate at on-top and hollow sites of underneath graphite or metal layers for OT1 and

OT2, respectively. Bridge configurations (BR), corresponding to the formation of graphene epoxide, are identical in each system. We considered the relative position of a graphene sheet with respect to the metal substrate reported to be the most stable (Fig. 1d): half of the C atoms located at on-top sites of metal atoms and the other C atoms located at the fcc hollow site of (111) metal substrates. Atomic oxidation on graphene (−3.31 eV, BR), graphite (−3.30 eV, BR), and Gr/Cu(111) is exothermic (−3.82 eV, OT1) because of the high reactivity of atomic oxygen, consistent with previous computational results and experimental observations using atomic oxygen produced by thermal cracking of molecular oxygen. Whereas the formation of BR is more favorable on both graphene and graphite than adsorption at on-top sites (by ~0.9 eV), the adsorption site preference dramatically changes on the epitaxial graphene grown on Cu(111) substrates. On Gr/Cu(111), OT1 becomes more stable than BR by 0.10 eV, although OT2 is still less favorable than BR by 0.07 eV. These results imply that the interfacial interaction between graphene and metal substrate is crucial in accounting for the stability of O adsorbate. Considering the geometric difference between OT1 and OT2 (see Fig. 1), OT1 can achieve effective electronic coupling between the 2p state of C atoms and the 3d state of the metal substrate along the z-axis, especially at the β position, i.e., C atoms adjacent to C atom (α) bonding with O.

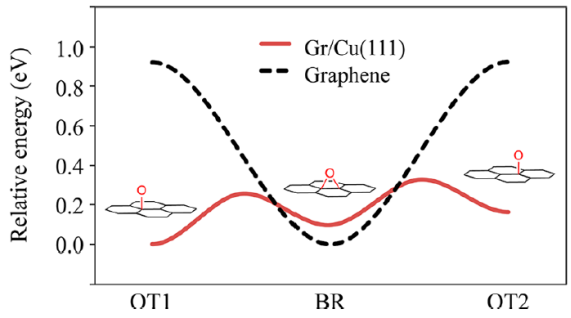

Figure 2. Potential energy surfaces for the oxygen migration between on-top (enolate) and bridge (epoxide) sites on free-standing graphene and Gr/Cu(111). The relative energy was used in constructing a potential energy surface.

We further examined the detailed potential energy surface for migration of O adsorbate between the on-top and bridge sites on the graphene sheet by means of CI-NEB calculations. Figure 2 clearly shows the existence of OT1 (and OT2) as a local minimum on Gr/Cu(111). The energy required for migration of O adsorbate on Gr/Cu(111), i.e., the potential energy barrier from OT1 to BR (from OT1 to OT2 through BR), is 0.26 (0.33) eV, much smaller than that on free-standing graphene (0.92 eV). Our results suggest that a novel chemical route for further functionalization of graphene grown on metal substrates, beyond isolated graphene and graphite, is possible.

To examine detailed interfacial interaction between graphene and metal substrate, we investigated the band diagrams of bare and OT1 Gr/Cu(111), and corresponding partial charge density plots at the **K**-point, as shown in Fig. 3. For bare Gr/Cu(111), the characteristic Dirac cone in the band structure of graphene at **K** is well preserved due to physisorption, and its conical point locates at the −0.41 eV with respect to the E_F (Fig. 3a). Figures 3c and 3d show the partial charge density for degenerated electronic states at the Dirac conical point, which indicates that the C 2p states of graphene are isolated from the electronic states of Cu(111). However, the electronic structure of bare Gr/Cu(111) is significantly modified by the formation of enolate on the basal plane, as shown in Fig. 3b. First, the calculated band structure shows a band gap opening of 0.18 eV. Second, the interfacial electronic couplings are strongly enhanced, as shown in Fig. 3f–h, which implies that the interfacial interaction between graphene and Cu(111) changes from physisorption to chemisorption. In particular, Figures 3f and 3g clearly show that the 2p states of β C atoms strongly interact with the 3d states of underlying Cu atoms at the interface.

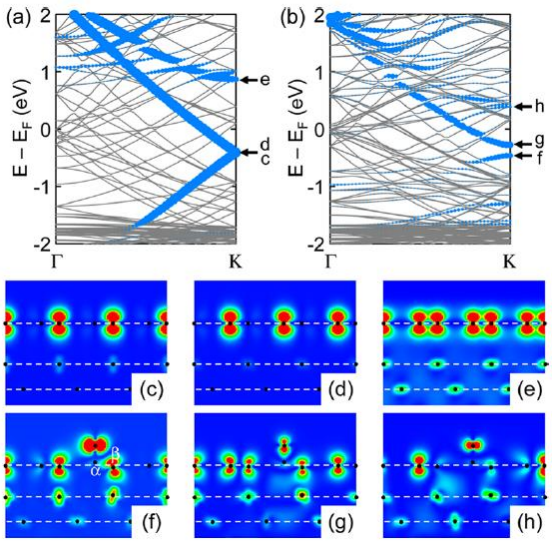

Figure 3. Band diagrams of (a) bare and (b) OT1 Gr/Cu(111). The relative amount of C 2pz character is proportional to the size of the blue dots. (c–h) Partial charge density plots for selected electronic states at **K**, for which energies are marked by black arrows in (a) and (b). Color grid for the probability of finding the electrons ranges from 0.000 (blue) to 0.005 (red) e/bohr^3. Black dots indicate the atomic positions.

In addition, we extended our study to epitaxial graphene grown on a Ni(111) substrate, Gr/Ni(111). Cu(111) and Ni(111) are representative metal substrates that interact weakly and strongly with graphene, respectively. The geometric and electronic structures associated with atomic oxidation of Gr/Ni(111) are quite complicated compared to those for Gr/Cu(111) due to the strong chemisorption at the interface. Our DFT calculations revealed, however, that the formation of enolate is possible on Gr/Ni(111), like that on Gr/Cu(111). The adsorption energies (relative energies) of atomic oxygen on Gr/Ni(111) are −4.59 (0.00), −4.16 (0.43), and −4.10 (0.49) eV for OT1, BR, and OT2, respectively, and they are all local minima. The stability order of atomically oxidized Gr/Ni(111) is identical to that in Gr/Cu(111). The much enhanced stability of OT1 on Gr/Ni(111) compared with Gr/Cu(111) also suggests that the interfacial interaction plays a crucial role in determining the structure of atomically oxidized graphene because of the ability of Ni(111) to have a stronger interfacial interaction with graphene. Our results for both Gr/Cu(111) and Gr/Ni(111) imply not only that the formation of enolate can be reasonably achieved in graphene grown on metal substrate through atomic oxidation but also that the properties of functionalized graphene can be controlled by the choice of metal substrate.

To summarize, our computational results strongly suggest that atomic oxidation of graphene grown on a metal substrate can provide an opportunity to extend graphene chemistry with a newly suggested functional group, enolate, on the basal plane of graphene. The interfacial interaction between graphene and metal substrate plays a crucial role not only in the formation of enolate as a local minimum but also in stabilizing it over the epoxide. Our computational study is expected to trigger experimental attempts to find the existence of graphene enolate on metal substrates and to design new chemical pathways utilizing it.

(2) Thermally activated polymorphic transition from 1D ribbon to 2D carpet: squaric acid on Au(111)

Polymorphic transitions of molecular assemblies on solid surfaces have recently attracted great interest for developing organic-based functional devices. The polymorphic transition has so far been extensively studied in supramolecular assemblies at the liquid–solid interfaces. However, ultrahigh-vacuum (UHV) conditions provide a different approach to fabricate “solvent-free molecular assembly” and to control its morphological and physical properties. The polymorphic transition of molecular assembly under UHV is, therefore, of importance for gaining fundamental insights into the underlying mechanism based on molecule–substrate and/or intermolecular interactions without involving solvent molecules. Intermolecular interactions such as hydrogen bonding (H-bonding) and van der Waals (vdW) interactions, balanced with

molecule-substrate interactions, are generally considered to play an important role in engineering molecular arrangements on solid surfaces. To the best of our knowledge, only a few studies have been reported on the polymorphic transition under UHV conditions with respect to the dimensionality of molecular assembly on solid surfaces, despite the importance of structural versatility in designing molecular assembly as a building block for ultimate device miniaturization.

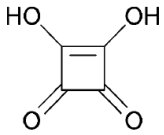

Scheme 1. Squaric acid (3,4-dihydroxycyclobut-3-ene-1,2-dione).

In this study, we demonstrate the polymorphic transition from a 1D ribbon to a 2D carpet superstructure of squaric acid (H2SQ, see Scheme 1) molecules on a Au(111) surface through a thermally activated process, using STM and DFT calculations. Our study revealed that the stability of the conformational isomers and assembled structures is crucial for determining the dimensionality of the 1D ribbon and 2D carpet H2SQ superstructures, respectively. We employ a simple H2SQ molecule as a prototype system that forms a layered structure with strong H-bonding. All the STM images were obtained using a low-temperature scanning tunneling microscope at 5 K in a UHV condition.

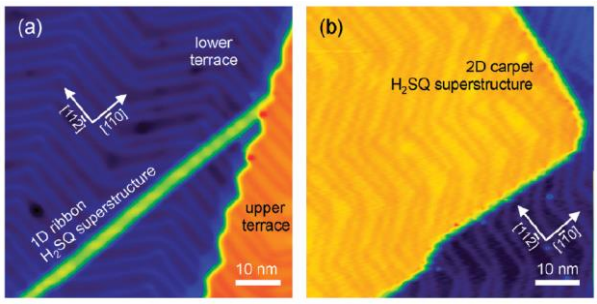

Figure 4. STM images (65 × 65 nm^2) of (a) the as-deposited 1D ribbon (V_s = 500 mV, I_t = 0.25 nA) and (b) the 2D carpet H2SQ superstructure after annealing at ~320 K for 5 min (V_s = 400 mV, I_t = 0.3 nA).

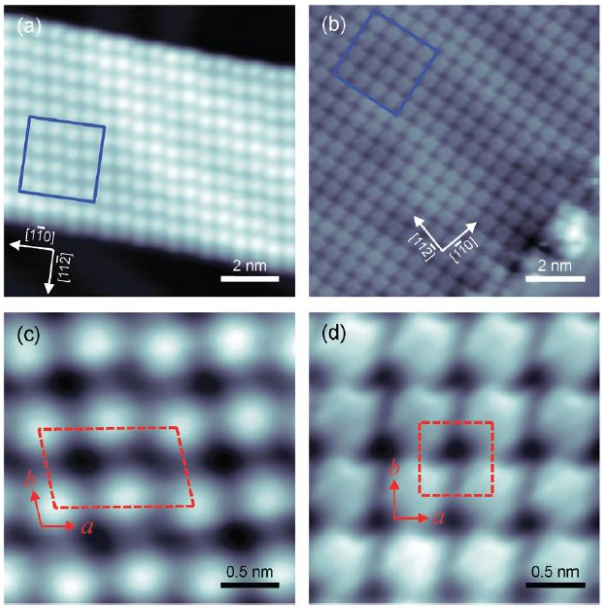

Figure 5. Molecularly resolved STM images of (a) 1D ribbons (V_s = 250 mV, I_t = 0.3 nA) and (b) 2D carpet (V_s = 25 mV, I_t = 0.3 nA) H2SQ superstructures on a Au(111) surface. Magnified STM images of blue squares in (a) and (b) are presented in (c) and (d), respectively. Unit cells of both structures are indicated by red-dashed lines.

Figure 4 shows the STM images of two types of H2SQ molecular superstructures formed on Au(111). The narrow 1D ribbon superstructure was observed after depositing H2SQ molecules onto Au(111) at RT (Fig. 4a). Subsequent thermal annealing at ~320 K resulted in a polymorphic transition to the 2D carpet superstructure (Fig. 4b). It should be noted that the polymorphic transition did not involve additional deposition of H2SQ molecules, despite a significant difference in the local coverage between 1D and 2D superstructures shown in Figs. 4a and 4b. Whereas the 1D superstructure presents a fully anisotropic morphology with a high length-to-width aspect ratio, the 2D superstructures are close to an isotropic square island with a size of several thousands of nm^2. Figure 5 shows the molecularly resolved STM images, which not only show uniform molecular electronic structures but also provide a view of the detailed molecular arrangements inside the 1D ribbon (Fig. 5a) and 2D carpet (Fig. 5b) superstructures. The blue square regions of Figs. 5a and b were enlarged, as shown in Figs. 5c and 5d,

respectively. The unit cells reveal the different molecular arrangements, i.e., anisotropic parallelogrammic arrangement for 1D (Fig. 5c) and isotropic square arrangements for 2D (Fig. 5d) H2SQ superstructures.

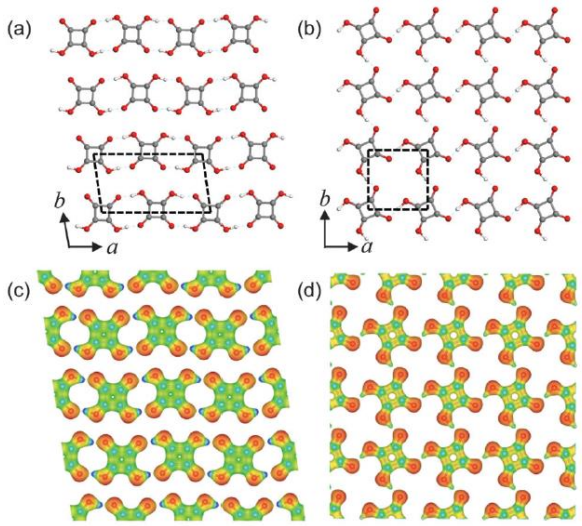

Figure 6. Optimized structures of (a) 1D ribbons and (b) 2D carpet H2SQ superstructures (C, gray; H, white; O, red), corresponding to Figs. 2c and 2d, respectively. Electrostatic potential maps of 1D and 2D superstructures are presented in (c) and (d), respectively. The relative color scale of electrostatic potential maps from red to blue corresponds to the negative to positive region on the molecular surface.

To interpret the experimental results obtained using STM, we carried out extensive periodic DFT calculations with a variety of molecular arrangements. We used the DFT-D2 method to fully consider the intermolecular interactions, including the vdW forces. Based on the incommensurate molecular arrangement for both 1D and 2D H2SQ superstructures on Au(111), indicating weak molecule-substrate interactions, we performed DFT calculations considering only the molecular configurations without the substrate. The optimized structures corresponding to the 1D ribbon (Fig. 5c) and 2D carpet (Fig. 5d) H2SQ superstructures are presented in Figs. 6a and 6b, respectively. Our calculations revealed that the 2D superstructure is more stable than the 1D superstructure by 0.12 eV per one H2SQ molecule. Therefore, the polymorphic transition from the 1D to 2D superstructure by thermal annealing, as observed in our STM experiments, can be clearly explained by the higher stability of the 2D carpet superstructure. Interestingly, the two H2SQ superstructures on Au(111) are composed of different conformational isomers (Figs. 6a and 6b). Isolated H2SQ molecule has five conformational isomers depending on the relative position of the two H atoms, in which the most stable two isomers are ZZ (C_{2v}) and EZ (C_s). Figure 6 shows that the less stable 1D structure compared to the 2D structure consists only of ZZ isomers, which are more stable than EZ isomers in the gas phase. In contrast, after annealing, the 2D structure is composed of only EZ isomers. These results indicate that different driving forces induce the formation of the two superstructures. The initial formation of the 1D superstructure at RT is determined by the relative monomeric stability among the H2SQ isomers in the gas phase, and the polymorphic transition from the 1D to 2D superstructure by annealing can be explained by a change in the overall stabilization mechanism from the stability of individual monomers to the stability of the assembled structure. The main intermolecular interaction in both superstructures can be considered to be H-bonding (Fig. 6). The H-bonding distance within the 2D molecular arrangement is calculated to be 1.33 Å, which is considerably shorter than that in the 1D superstructure (1.43–1.47 Å). As a consequence, the 2D superstructure achieves a more effective intermolecular H-bonding network compared to the 1D superstructure, during the annealing process. In addition to H-bonding interactions, we can consider vdW interactions within the 1D molecular arrangement (Fig. 6a), where the neighboring molecular rows, entangled by H-bonding along the *a*-axis, are interlocked by the vdW interactions along the *b*-axis. To study the influence of intermolecular interactions on a molecular arrangement in more detail, we plotted the electrostatic potential maps for both the 1D and

2D superstructures in Figs. 6c and 6d, respectively. While attractive H-bonding is found in the 2D superstructure in an isotropic manner (Fig. 6d), electrostatic repulsion between the neighboring molecular rows in the 1D superstructure (Fig. 6c) causes a gradual shift in the position of the molecular rows along the *a*-axis, which causes not only the distortion of the rectangular arrangement but also the alternative displacement of the molecular center from the axis of the molecular rows.

In summary, we have demonstrated the thermally activated polymorphic transition from the 1D ribbon to 2D carpet superstructures using H2SQ molecules on Au(111) under UHV through STM experiments combined with DFT calculations. We found that the molecular arrangements in the 1D ribbon and 2D carpet superstructures are determined by the stability of the conformational isomers and assembled structures, respectively.

(3) Supramolecular assembly through interactions between molecular dipoles and alkali metal ions

There have been numerous attempts to form well-ordered organic monolayers by employing intermolecular covalent bonding, H-bonding, electrostatic interactions, and vdW interactions. Metal–ligand networks, which use metal adatoms for binding molecules, are also useful to form well-ordered assemblies spontaneously. Chemical modification of molecules with functional groups that can serve as ligands such as cyanide, isocyanide, carboxylate, and pyridine, lead to substantial interaction with metal adatoms to form both 2D networks and 1D chains on metal substrates. Although rigid frameworks can be constructed by this method, the strong chemical bonding between metal and ligand that forms an organometallic complex may give rise to a significant change in intrinsic functional properties of the molecule. One potential strategy to simultaneously achieve the preservation of desired molecular properties and the fabrication of a stable molecular superstructure is conceived to use weak ion-dipole interactions, which are yet stronger than dipole-dipole and vdW interactions. Diarylethene (DAE) could be one of the candidates to achieve supramolecular assembly through ion-dipole interactions, because it has an intrinsic dipole resulting from its unique structure (Scheme 2) and has no functional groups acting as a ligand with metal ions. DAE is well-known for its photochromism, and thus switching properties as well as optoelectronic and optomechanical applications have been intensively studied.

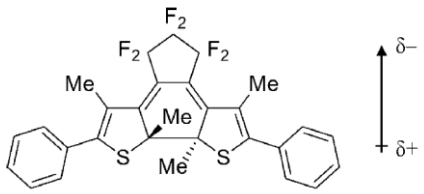

Scheme 2. Structure of DAE molecule used in this study and the orientation of the molecular dipole moment. Calculated molecular dipole moment of the isolated molecule is 5.83 D.

Herein, we report the successful formation of a metal ion-DAE superstructure using a simple DAE molecule on the Cu(111) surface by co-deposition of NaCl followed by mild annealing. Based on STM and DFT calculations, we propose a possible model for the superstructure, which consists of Na^+ ions and closed-form isomers of DAE. The driving force for the superstructure formation is indeed suggested to be ion-dipole interactions between Na^+ ions and the DAE molecules, which results in a row-type molecular arrangement along the molecular dipole axis.

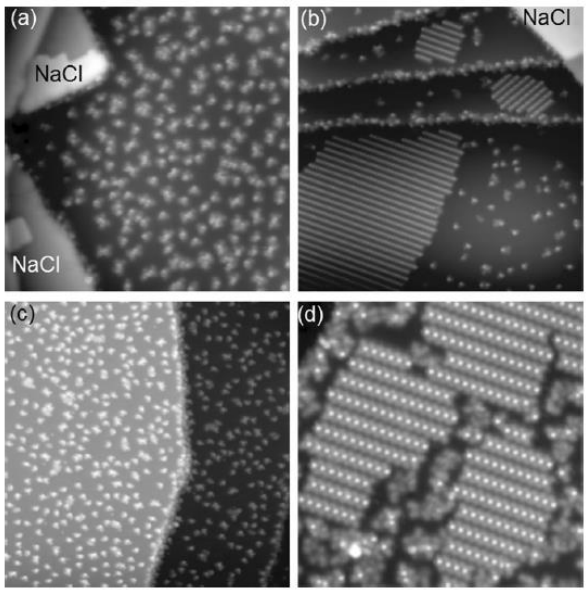

Figure 7. STM images of closed-form DAE adsorbed on Cu(111) at RT with pre-deposited NaCl islands, (a) before and (b) after annealing. (c) Closed-form isomers adsorbed on clean Cu(111) at RT followed by annealing. (d) DAE superstructure prepared by deposition of the closed-form isomer followed by deposition of NaCl and annealing. Image sizes: a) 50×50 nm^2, b,c) 80×80 nm^2, and d) 30×30 nm^2. Tunneling conditions: a,b) V_s = –2 V and I_t = 50 pA, c) V_s = +2 V and I_t = 100 pA, d) V_s = +1 V and I_t = 30 pA.

Deposition of the closed-form isomer of DAE on the Cu(111) surface with pre-adsorbed NaCl islands under UHV condition leads to a random distribution of adsorbed molecules on Cu(111), as shown in Fig. 7a. All DAE molecules were found on clean Cu(111) regions and the rims of NaCl islands, and no molecules were adsorbed on the NaCl islands due to the smaller adsorption energy of DAE on top of the NaCl islands compared to that on Cu(111). After annealing the sample at ca. 360 K, well-ordered molecular films, which are composed of linear molecular rows, appeared on the Cu terraces (Fig. 7b). Three equivalent orientations of the row structure (two are shown in Fig. 7b), along the $\langle 11\bar{2} \rangle$ directions of Cu(111), were found. The co-deposition of NaCl is essential for the formation of a well-ordered DAE superstructure on Cu(111). Without NaCl, the molecules remained randomly adsorbed as isolated monomers, dimers, or small clusters even after annealing (Fig. 7c). By post-depositing NaCl on the DAE/Cu(111) surface followed by annealing at ca. 360 K, we were able to fabricate molecular films (Fig. 7d) that were identical to those formed by DAE deposition with pre-adsorbed NaCl islands (Fig. 7b). These observations strongly indicate the necessity of Na, Cl, or both for superstructure formation.

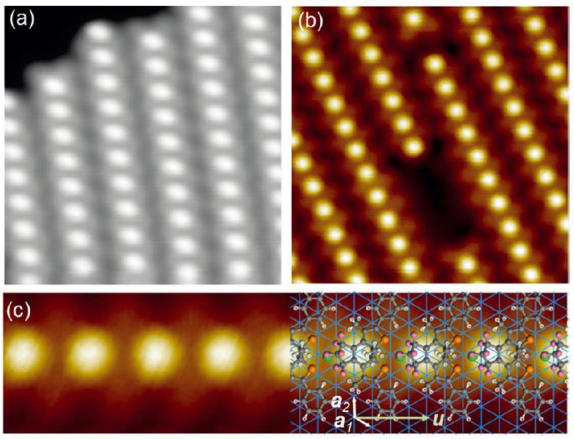

Figure 8. (a) STM image (10×10 nm^2) of the edge region of the superstructure. (b) STM image (9×9 nm^2) containing a vacancy (one missing molecule) and void (four missing molecules). (c) Proposed superstructure model superimposed on the enlarged, rotated, and trimmed STM image from (b). Unit vectors of the Cu(111) surface and one of the unit vectors of the superstructure are indicated. Tunneling conditions: V_s = +1 V and I_t = 30 pA.

All molecules are triangular with a bright spot at the center, and the DAE molecules within a molecular row adsorb in the identical structure with the same orientation; however, adjacent rows have opposite molecular orientations, as clarified by imaging the edges of the molecular film (Fig. 8a) as well as the vacancies and voids within the films (Fig. 8b). Based on the STM contrast of the closed-form DAE and orientation of the Cu(111) lattice, we constructed a model of the superstructure, as displayed in Fig. 8c. The model uses the optimized structure of a single DAE row, which will be described in detail below. The basis vectors of the unit cell in the DAE superstructure, u and v, are defined as u=4a_1+2a_2 and v=15a_2, respectively, in which a_1 and a_2 are the unit vectors of the Cu(111) lattice. Several groups

have reported molecular superstructure formation through co-deposition of alkali halides. For molecular films of tetracyanoquinodimethane (TCNQ) on Au(111) and terephthalic acid (TPA) on Cu(100) with NaCl co-deposition, the molecular packing geometries differ from those formed in the absence of alkali halides. In these previous reports, the observed superstructures were concluded to be molecule-alkali metal ionic crystals, and the disappearance of Cl was evidenced by the reduction of the Cl 2p peak during in situ X-ray photoelectron spectroscopy (XPS). Our XPS experiments also support the idea that Na binds to DAE and Cl disappears from the surface because of the penetration into the bulk.

Periodic DFT calculations were carried out to gain insight into the formation of the DAE superstructure on Cu(111); we focused on the driving force leading to the anisotropic geometric configuration of the molecular film, i.e., the formation of a row structure. Therefore, we employed a supercell for an isolated single DAE molecular row, i.e., $b_1=4a_1+2a_2$ and $b_2=10a_2$, in which the smallest atomic distance between adjacent molecular rows was ca. 10 Å. We also investigated the role of the incorporated Na^+ ions in the formation of the molecular rows to explain our experimental findings, i.e., the successful fabrication of a DAE superstructure only with NaCl co-deposition. Extensive geometry optimizations were performed to obtain the most stable structure using the initial geometrical configurations of combinations of three adsorption orientations (i.e., P1, P2, and P3 according to the molecular plane facing the Cu(111) surface, as shown in Fig. 9a) and four adsorption sites (on-top, bridge, fcc and hcp hollow sites according to the position of the center of mass of the DAE molecule).

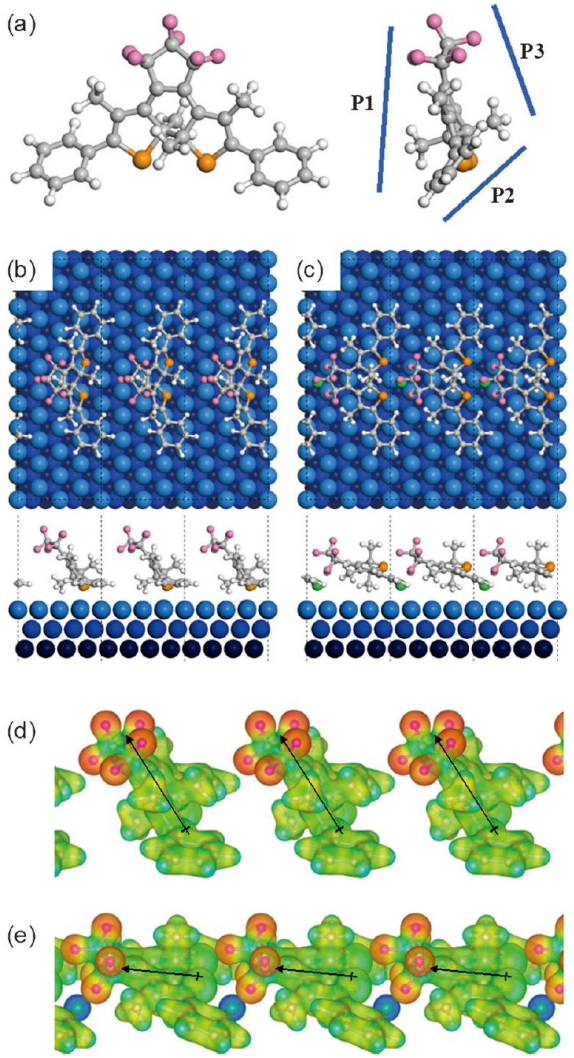

Figure 9. (a) Ball-stick model of closed-form DAE. On the right-hand side, a side view of the molecule and the three planes facing the Cu(111) surface considered in the calculations are shown; color code: gray C, white H, pink F, orange S. Top and side views of the DFT-optimized DAE row structure (b) without and (c) with Na^+ (green). (d and e) Side views of the electrostatic potential maps of (b) and (c), respectively. Blue to red corresponds to positive to negative charges. Black arrows represent the molecular dipoles. Calculated molecular dipole moments for (d) and (e) are 10.11 D and 7.51 D, respectively.

Figures 9b and 9c show the most stable optimized structures for the molecular rows without and with Na^+ ions between neighboring DAE molecules, respectively. In both cases, the hcp hollow site is the most stable adsorption site. Figure 9c displays a drastic change in adsorption geometry from that in Fig. 9b because of the presence of Na^+ ions in the molecular row. Whereas the upright adsorption

orientation (P2) of DAE molecules on Cu(111) is preferred in the absence of Na^+ ions (Fig. 9b), the flat-lying adsorption orientation (P1) is the most stable in the presence of Na^+ ions (Fig. 9c). In the absence of Na^+ ions, two sulfur atoms of the DAE molecule interact mainly with the Cu substrate; this is also accompanied by vdW interactions between the phenyl rings and the substrate. Thus, the DAE molecules should be oriented in the upright adsorption configuration. In contrast, when Na^+ ions are inserted between neighboring DAE molecules, the adsorption orientation in the molecular row is significantly altered, in which the Na^+ ions adsorbed on Cu(111) strongly interact with two fluorine atoms of DAE and thus draw the electronegative part of the DAE molecule closer to the substrate. Figures 9d and 9e show the electrostatic potential maps for isolated single DAE molecular rows without and with Na^+ ions, respectively, which clearly indicate that the attractive electrostatic interactions between Na^+ ions and DAE molecules modify the direction of the molecular dipole moment to be parallel to the substrate.

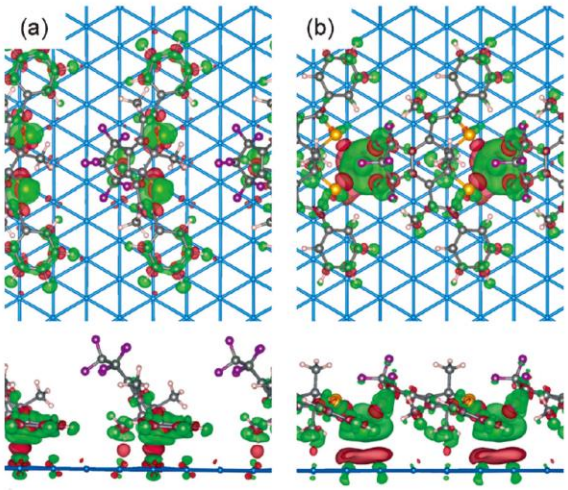

Figure 10. Top and side views of the charge density difference maps for the DFT-optimized DAE row structures (a) without and (b) with Na^+.

As a proof of ionization of the Na atoms on the Cu(111) surface, we show in Figs. 10a and 10b the charge density difference maps for the molecular row without and with Na, respectively. Depletion of the charge around Na is clearly depicted (Fig. 10b), and the net charge of Na is found to be +0.77*e*. The ion–dipole interactions along the axis of the molecular row also compensate for the reduced interfacial interaction between the DAE molecules and the Cu(111) substrate. Therefore, our computational results strongly suggest that the ion-dipole interactions induced by Na^+ ions play a crucial role in the formation of an anisotropic geometric configuration, i.e., the formation of row structures along the axis of the ion-dipole interactions. The overall energy gain by Na incorporation along the molecular row in the superstructure, which is accompanied with charge redistribution, is found to be 0.64 eV per one DAE molecule.

In conclusion, we demonstrated the formation of a well-ordered superstructure of photochromic DAE molecules on Cu(111) by means of vacuum evaporation of either isomer with NaCl co-deposition followed by mild annealing. Na^+ incorporation is evident from a comparison of experimental STM images with DFT calculations. The key to the superstructure formation with anisotropic geometric configuration, i.e., the formation of a linear row structure, is suggested to be ion–molecule dipole interaction. Our results demonstrate a potential strategy to utilize alkali metal co-deposition to simultaneously control electronic properties and tune intermolecular interactions.

(4) Orbital-selective Kondo effect control via coordination chemistry

Iron(II) phthalocyanine (FePc) molecule causes novel Kondo effects derived from the unique electronic structure of multi-spins and multi-orbitals when attached to Au(111). Two unpaired electrons in the dz^2 and the degenerate dzx/dyz orbitals are screened

stepwise, resulting in spin and spin+orbital Kondo effects, respectively. We investigated the impact on the Kondo effects of the coordination of CO and NO molecules to the Fe^{2+} ion as chemical stimuli by using STM and DFT calculations.

All the STM experiments were performed at the sample temperature of 0.4 ~ 2.6 K in an UHV chamber (base pressure of 5×10^{-11} Torr). An electrochemically etched W wire was used as the STM tip. All the STM images were acquired by constant current mode with a bias voltage V_s applied to the sample. The first derivative of the tunneling current I_t (dI/dV) was measured as a STS spectrum with a lock-in technique where the modulation voltage (V_{mod} = 0.06 mV and frequency f = 312.6 Hz) was overlapped to V_s with the feedback loop switched off. The evolution of the Kondo resonance with magnetic field was measured by using two superconducting magnets which generate the magnetic fields parallel and perpendicular to the sample surface. The DFT calculations were performed by using the plane-wave-based VASP with the PAW method. The exchange and correlation were described at the level of LDA. We used the exchange-correlation functional determined by Ceperly and Alder and parameterized by Perdew and Zunger. The strong correlation effects in the d-electron states of the Fe atom were treated by the LDA+U method with U = 2.0 and J = 1.0 eV. These values of U and J were determined by comparing the energy spectrum calculated for an isolated FePc molecule with that measured for the bulk FePc. The CO- or NO-coordinated FePc complex (hereafter we call them CO- and NO-FePc, respectively) on Au(111) was modeled by (8×8) supercell, which consists of an CO- or NO-FePc on a 3-layer Au slab with a vacuum of ~15.6 Å thick along the surface normal. The positions of atoms in both coordinated complex and outermost two layers of Au slab were optimized without any constraint until the forces on individual atoms were less than 0.02 eV/Å. Because of the large dimensions of the supercell, the Brillouin zone was sampled with a single k-point only at Γ point.

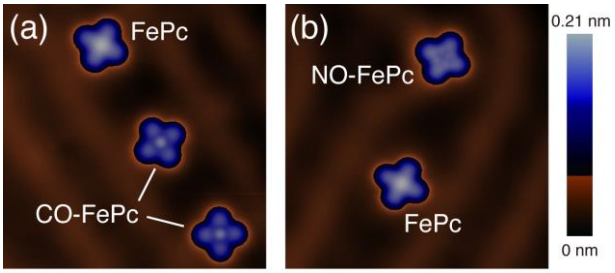

Figure 11. STM topographic images of (a) CO- and (b) NO-FePc on Au(111)

Figures 11a and 11b show topographic STM images of CO- and NO-FePc complexes on Au(111), respectively. The complexes appear as a cross similarly to the FePc molecule free from CO or NO.

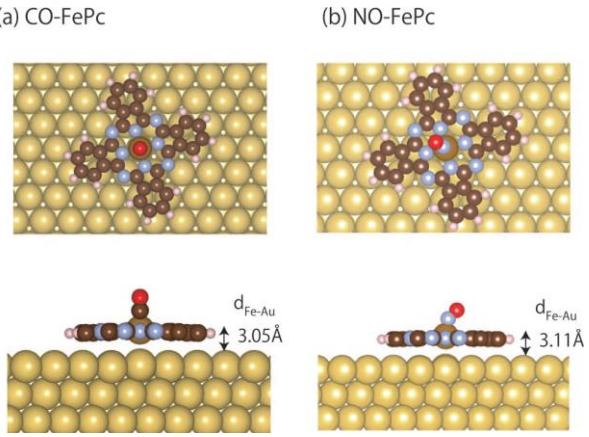

Figure 12. Structure models of (a) CO-FePc and (b) NO-FePc on Au(111) optimized by DFT calculations. The upper and lower drawings are top and side views, respectively. These models are generated by VESTA.

The stable coordination structures of the CO- and NO-FePc complexes were determined by the DFT calculations as shown in Figs. 12a and 12b, respectively. The CO molecule adsorbs upright in the central Fe^{2+} ion (Fig. 12a). In contrast, the NO molecule adsorbs at the Fe^{2+} ion with the molecular axis tilting toward the N atom at the periphery of the C-N-C conjugated ring (Fig. 12b). Reflecting the symmetry of FePc, the NO-FePc complex has four energetically-equivalent configurations. The impact

of the coordination on the geometric structure is observed in the bond length of Fe and Au underneath. The bond length is elongated from 2.69 Å in FePc to 3.05 Å in CO-FePc and 3.11 Å in NO-FePc, indicating that the coordination of CO and NO reduces the coupling of the complex with the substrate.

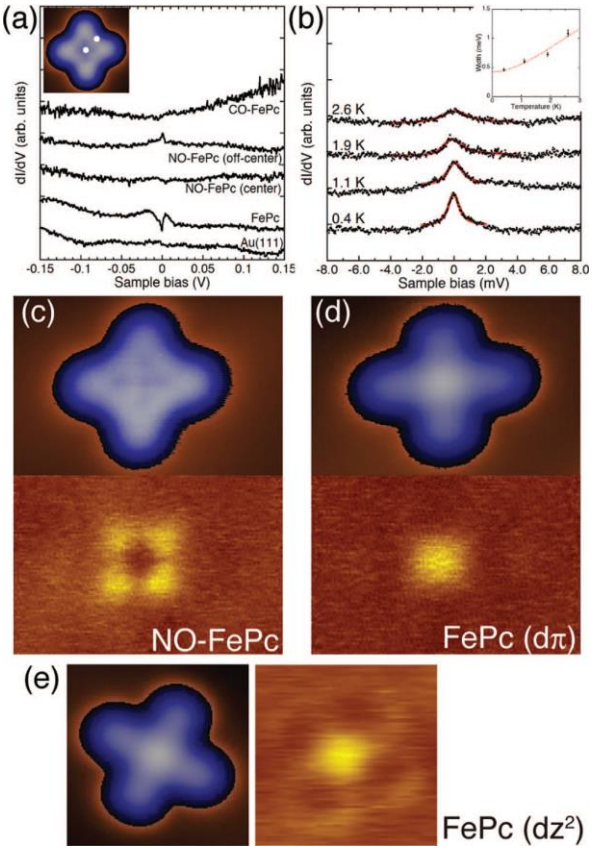

Figure 13. (a) The STS spectra of FePc, CO-FePc and NO-FePc. The spectra of FePc and CO-FePc were taken by holding an STM tip over the centers. A broad peak and a sharp dip observed for FePc are associated with the Kondo resonances. The spectra of NO-FePc were taken at the center and the off-center as shown in the inset. A sharp peak appears in the spectrum taken at the off-center while the spectrum is flat measured at the center. (b) The temperature evolution of the sharp peak observed for NO-FePc. The red lines are calculated by the Fano function. The inset shows the temperature variation of the peak width. The STS maps of the Kondo resonances of (c) NO-FePc, (d) FePc (dzx/dyz and (e) FePc (dz^2) together with the topographic images measured simultaneously.

The coordination of CO drastically changes the Kondo signatures observed for the FePc molecule free from CO on Au(111). For the FePc molecule in the ontop configuration, two Kondo resonances emerge due to the exchange couplings of molecular localized spins with the substrate electrons. A broad peak and a sharp dip appear in the STS spectrum as shown in Fig. 13a. The peak structure arises from the Kondo correlation of an electron in the dz^2 orbital, and the dip structure comes from the Kondo effect associated with electrons occupying the degenerate dzx/dyz orbitals. When the FePc molecule is coordinated with CO, both peak and dip disappear and the spectrum does not show any noticeable structures. In contrast to CO, the coordination of NO provides the different impact on the Kondo effects of FePc. Although both broad peak and sharp dip disappear similarly to CO-FePc, a sharp peak is observed at the E_F instead when FePc is reacted with NO (Fig. 13b). Similarly to CO-FePc, the NO molecule was removed by applying a pulsed voltage without any damage. The spectral change between FePc and NO-FePc was reversible. The sharp peak shows temperature dependence. Increasing the temperature, the peak becomes broader and more depressed as shown in Fig. 13c. We fitted the spectral shape with Fano function and obtained the peak width as a function of temperature T. The temperature evolution is fitted well as shown in the inset of Fig. 13b, indicating the origin of the peak is the Kondo resonance. The spatial distribution of the sharp peak observed for NO-FePc is different from those for FePc (compared to Figs. 13c, 13d and 13e). The spatial distribution of the sharp peak for NO-FePc shows a four-lobed pattern with the low intensity at the center (Fig. 13c). This contrasts to that of the dip structure observed for the FePc molecule in which the spectral intensity is observed at the molecular center (Fig. 13d).

Calculated spin-resolved electronic structure of NO-FePc uncovers the origin of the Kondo peak observed for NO-FePc as shown in Fig. 14. The spin polarization still survives because the NO molecule originally has an unpaired electron in the $2\pi^*$ MO.

The spin polarizations in the dzx/dyz orbitals are strongly depressed by the coordination of NO compared to FePc on Au(111). In contrast, a sizable splitting survives in the dz^2 orbital. A sharp peak appears at –0.5 eV below the E_F for the majority spin while the counterpart is observed at +0.4 eV above the E_F for the minority spin. Thus, the spin polarization survives in the dz^2 orbital. Furthermore, the peaks observed at –0.5 and +0.4 eV relative to the E_F are much sharper compared to FePc on Au(111). This sharpening indicates the weak bonding interactions between Fe and Au underneath.

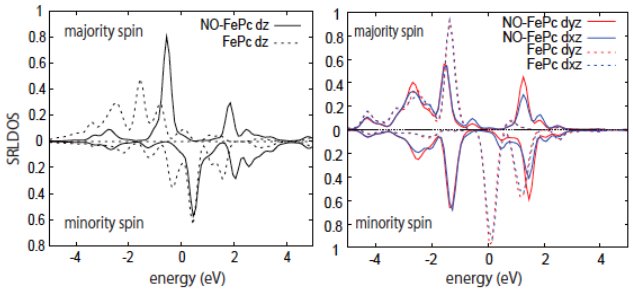

Figure 14. Spin-resolved local density of state (SRLDOS) spectra projected onto the dz^2 and dzx/dyz orbitals calculated for NO-FePc. The SRLDOS spectra of FePc are also shown with dashed lines for comparison.

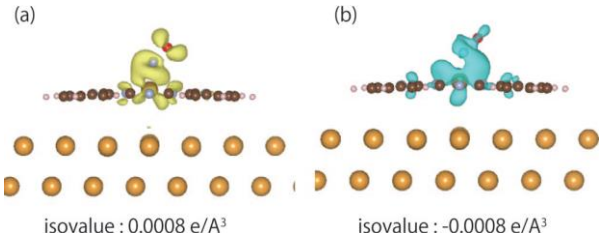

Figure 15. The spatial distribution of spin density in the molecular orbital relevant of the Kondo effect in NO-FePc. The figure is generated by VESTA.

The four-lobed pattern observed for the Kondo peak of NO-FePc (Fig. 13d) is rationalized by the combination of the spatial distribution of the orbital having the impurity spin with the tunneling probability of electrons. In the NO-FePc complex, the impurity spin exists in the molecular orbital consisting of the 5σ, 2π* and dz^2 orbitals. Figure 15 shows the spatial distribution of spin density in this molecular orbital. The spin density is high at the central Fe region, which extends to the N and O atoms of NO molecule. Considering the rotation of NO, the spectral distribution reflects the superposition of the spin distributions of the four equivalent tilting configurations. This partly explains the four-lobed pattern, but hardly explains the low intensity at the center of the complex. This can be rationalized by considering the tunneling probability. The O atom is the closest to the STM tip, and thus the tunneling probability is high. In addition, this orbital has a node between the N and the O atoms, which is positioned nearly above the Fe region. This node prohibits the electron tunneling into the central region of NO-FePc, leading to the low intensity in the spectral distribution. The combination of the orbital shape responsible for the Kondo resonance with the spatially-variable tunneling probability explains the four-lobed pattern. This idea is also supported by the topographic image of NO-FePc. The dark cross is observed in the various tunneling conditions. This indicates that the tunneling takes place mainly through the electronic states at the O atom of rotating NO.

In summary, we investigated the geometrical and electronic structures of CO- and NO-FePc complexes on Au(111) and how the coordination of CO and NO gives impact on the Kondo effects of FePc on Au(111) by STM combined with the DFT calculations. When FePc is coordinated with CO or NO, the CO takes an upright configuration while the NO favors a tilting configuration. The impacts of CO and NO to the spin and Kondo effects are different from each other. Upon the coordination of CO, the localized molecular spins disappear due to the change in electron configuration by the formation of chemical bond between Fe and CO. In case of the NO coordination, the Kondo resonance derived from the dz^2 orbital is modified and the Kondo temperature is drastically lowered because the coupling of Fe and the substrate

is reduced.

4. Conclusions

We have tried to examine a variety of molecular behaviors on the surface in FY2014. (1) We first suggested that atomic oxidation of graphene grown on a metal substrate results in the formation of graphene enolate, i.e., negatively charged oxygen adsorbed at the on-top position on its basal plane, which is strikingly different from the formation of epoxy groups on free-standing graphene and on graphite. Whereas the enolate is the transition state between two neighboring epoxides on free-standing graphene and on graphite, we revealed that the enolate group formed on epitaxial graphene on a metal substrate exists as a local minimum, and further becomes more stable than the epoxide. (2) We demonstrated the thermally activated polymorphic transition from the 1D ribbon to 2D carpet superstructures using H2SQ molecules on Au(111) under UHV through STM experiments combined with DFT calculations. We found that the molecular arrangements in the 1D ribbon and 2D carpet superstructures are determined by the stability of the conformational isomers and assembled structures, respectively. (3) We demonstrated the formation of a well-ordered superstructure of photochromic DAE molecules on Cu(111) by means of vacuum evaporation of either isomer with NaCl co-deposition followed by mild annealing. Na^+ incorporation is evident from a comparison of experimental STM images with DFT calculations. The key to the superstructure formation with anisotropic geometric configuration, i.e., the formation of a linear row structure, is suggested to be ion–molecule dipole interaction. (4) We investigated the geometrical and electronic structures of CO- and NO-FePc complexes on Au(111) and how the coordination of CO and NO gives impact on the Kondo effects of FePc on Au(111) by STM combined with the DFT calculations. When FePc is coordinated with CO or NO, the CO takes an upright configuration while the NO favors a tilting configuration. The impacts of CO and NO to the spin and Kondo effects are different from each other. Upon the coordination of CO, the localized molecular spins disappear due to the change in electron configuration by the formation of chemical bond between Fe and CO. In case of the NO coordination, the Kondo resonance derived from the dz^2 orbital is modified and the Kondo temperature is drastically lowered because the coupling of Fe and the substrate is reduced.

Our theoretical studies combined with experiments in FY2014 provide deep insight into a variety of chemical and physical phenomena on solid surface. We expect that our results can provide new perspective to develop a potential strategy for controlling electronic properties of molecular adsorbates on the surface.

5. Schedule and prospect for the future

(1) Controlling chemical reactivity of ultrathin oxide film

Ultrathin oxide film grown on metal substrate has been a subject of great interest not only as a supporting material for chemically active nanoparticles but also as a catalyst in the field of heterogeneous catalysis, where it provides various ways to control the properties of adsorbates via following factors (See Fig. 16): (i) charge transfer between adsorbates and oxide-metal interface, which is closely correlated with the electronic affinity (EA) of adsorbate and workfunction reduction, (ii) adhesion between oxide and metal layers with strong polaronic distortion, (iii) film thickness, and (iv) the chemical composition of oxide surface.

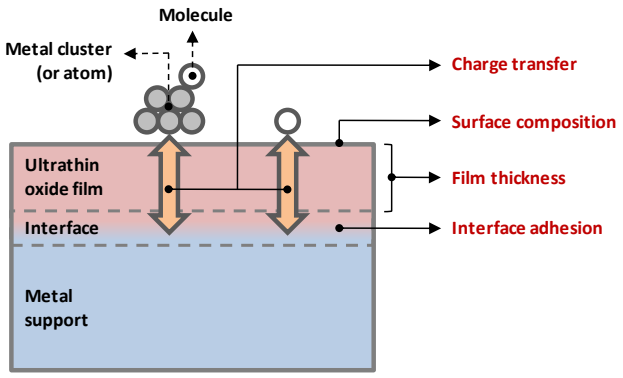

Figure 16. Schematic diagram for heterogeneous catalyst using ultrathin oxide film.

Therefore, we will continue our work to find the way for controlling the chemical reactivity using theoretical and experimental studies. In FY2015, we will extend our study into dissociation of CH_3OH and O_2 on MgO/Ag(100) using combined STM and DFT methodology. In particular, for O_2 dissociation on MgO/Ag(100), we should consider an influence from the charge redistribution between the oxide-metal interface and the adsorbate, because of O_2 has much higher EA than that of H_2O molecule. The other branch of our study is clear understanding of the drawing effect at the oxide-metal interface, which can enhance the concentration of dopants at the interface. In addition, we have interests in other ultrathin oxide film systems, such as titania and ceria. We believe that our study provides not only profound insight into the chemical reactivity control of ultrathin oxide film but also an impetus for investigating ultrathin oxide films for a wider range of applications.

(2) Molecular adsorption on solid surface: From single molecule to molecular network

The controllable fabrication of molecular architectures is a topic of great importance not only as a fundamental subject in surface science but also for realizing molecular-scale electronic devices. Computational techniques can provide the underlying mechanisms for the formation of various molecular architectures experimentally observed by STM as well as single molecule adsorption. For the adsorption of single molecules on metal substrate, we suggested the origin of adsorption-induced stability reversal of photochromic DAE on metal surfaces and revealed that the interfacial orbital interaction originated from the weak electronic coupling between the molecular π-state and the electronic states of the Au surface can play a decisive role in constraining adsorption geometry even in the archetypal vdW adsorption system. For one-dimensional (1-D) systems, we have explained (i) the formation mechanism of 1D zipper-type architecture of azobenzene derivatives with the balanced non-bonding interactions, H-bonding and vdW interactions, between adjacent molecules and (ii) the dispersive electronic feature due to the π-orbitals stacking in 1-D molecular lines fabricated on the Si(001)-(2×1)-H. For 2D systems, we contributed to unveil the adsorption geometry of 2D molecular films composed of fluorinated fullerene ($C_{60}F_{36}$), which is strongly related to the distribution of frontier molecular orbitals and thus the n-type character of molecular film. In addition, most recently we recently revealed the novel formation mechanism of supramolecular assembly using photochromic diarylethene derivative, which is the first report on molecular architectures formed by ion-dipole interaction on solid surface (see Fig. 9). Our results provide not only deeper insight into the molecular adsorption process, but also a general basis for designing the architectures of molecular electronics with desired electronic properties. In FY2015, we will continue the research not only for a variety of molecular assemblies but also isolated molecule on the surfaces as follows: (1) H2SQ derivatives on metal surface, (2) switching motion of azobenzenze derivatives on metal surface, (3) 2-D DNBA molecular assembly, and (4) phthalocyanine on insulating film surface.

(3) Electronic structures of functionalized graphene grown on metal substrate

Functionalization of graphene has attracted great scientific interest not only in controlling the physical properties of graphene, such as opening band gap to achieve semiconducting nature, but also in improving chemical adaptability to integrate graphene as a building block into a variety of functional devices. In particular, we first suggested that the atomic oxidation of graphene grown on a metal substrate results in the formation of graphene enolate, i.e., negatively charged oxygen adsorbed at ontop position on its basal plane, which is strikingly different from the formation of epoxy groups, i.e., adsorption of atomic oxygen at bridge position, on pristine graphene and on graphite (see Fig. 2). Whereas the enolate is the transition state between two nearest epoxides both on graphene and on graphite, we revealed that improved interfacial interaction between graphene and metal substrate during atomic oxidation plays a crucial role not only in the formation of graphene enolate as a local minimum but also in stabilizing it over the graphene epoxide (see Fig. 3). In FY2015, we are going to theoretically investigate our very recent experimental finding of well-ordered graphene functionalization, in which the formation of graphene enolate would be one of the main driving forces. Our results are expected to provide not only a novel perspective for a chemical route to functionalize graphene but also a new opportunity for graphene-based applications.

(4) Magnetism of molecule on solid surface

Magnetism of molecules has been investigated intensively due to their potential applications such as single molecular magnets and single molecular spin valves. In order to apply magnetic molecules to realistic devices, we need to place molecules in contact with solid surfaces. As series of studies have shown, depositing molecules on solid surfaces causes various effects such as charge transfer between molecules and surface which changes the electron states of molecules drastically. In addition, in order to discuss the magnetism in adsorbed molecules precisely, we need to treat many-body effects. This means that we have to construct a scheme which can treat the adsorption effects and many-body effect comprehensively. For this purpose, we try to combine the DFT calculations and quantum many-body theories. Specifically, we construct effective Hamiltonians based on DFT calculations results and solve them using quantum many-body theories.

From FY2012, we have investigated the Kondo effect in adsorbed molecules. In surface systems, the Kondo effect originates in the interaction between the localized spin of the adsorbate and the conduction electrons of the nonmagnetic metal surface. At low temperatures, the Kondo effect induces the formation of the characteristic ground state called as the Kondo singlet. Experimentally, this Kondo singlet can be observed as a sharp peak structure (Kondo peak) near the E_F in the STS spectra. In collaboration with STS experiments, we have found novel type of the Kondo effect in Fe-phthalocyanine (FePc) molecule on Au(111).

As further extension of these investigations, we focus on the functionalization of the substrate in FY2015. Recently, 2D materials can be fabricated on surface. Typical examples are graphene, and In atomic layer on Si(111). In these 2D systems, characteristic electronic structures such as Dirac electrons and monolayer superconductivity have been observed. The impact of these unique electronic states in 2D materials on molecular magnetism has never been investigated in detail. Therefore, we plan to clarify this point based on DFT calculation.

(5) Surface carrier dynamics in energy conversion processes

Dynamics of energetic carriers in semiconductors, such as scattering, recombination and diffusion, has attracted much attention from both fundamental and technological points of view. With recent advances in the field of nanotechnology, a deeper understanding of carrier dynamics at surfaces becomes more important. Recently, these behaviors in the electroluminescence processes can be investigated with atomic spatial resolution by using STM-induced light emission (STM-LE), where luminescence is induced by the tunneling current of STM. In FY2015, combining theoretical and experimental analyses, we will study the dynamics of energetic electrons at a (110) surface of GaAs that is one of the most important industrial materials used in optoelectronic devices. Since the presence of surface states in GaAs(110) would strongly affect the behavior of electrons, a detailed investigation of the electronic structure and electron dynamics at surfaces will reveal unprecedented phenomena that have never been recognized in the study of carrier dynamics in the bulk material. We plan to investigate this point using DFT calculation and an effective model calculation. It is expected that our study provide a novel insight into carrier dynamics in optoelectronic conversion processes of nanomaterials and aid in the design of novel materials for optoelectronic devices.

Fiscal Year 2014 List of Publications Resulting from the Use of RICC

* The members registered as the user of RICC system in FY2014 are indicated by underline.

[Publication]

1. J. Jung, H. Lim, J. Oh, and Y. Kim, "Functionalization of graphene grown on metal substrate with atomic oxygen: enolate vs epoxide", *J. Am. Chem. Soc.*, **136** (24), 8528 (Jun. 2014).

2. N. Tsukahara, E. Minamitani, Y. Kim, M. Kawai, and N. Takagi, "Controlling orbital-selective Kondo effects in a single molecule through coordination chemistry", *J. Chem. Phys.*, **141** (5), 054702 (Aug. 2014).

3. 南谷英美, 荒船竜一, 山本真祐子, 高木紀明, 川合眞紀, 金有洙,
   "光電子放出における電子-フォノン非弾性相互作用:Cu 表面におけるレーザー光電子スペクトルの解析", *表面科学*, **35** (8), 409 (Aug. 2014).

4. K. Ueji (§), J. Jung (§), J. Oh, K. Miyamura, and Y. Kim, "Thermally activated polymorphic transition from 1D ribbon to 2D carpet: squaric acid on Au(111)", *Chem. Commun.*, **50** (76), 19436 (Oct. 2014). [(§) equally contributing authors]

5. T. K. Shimizu (§), J. Jung (§), H. Imada, and Y. Kim, "Supramolecular assembly through interactions between molecular dipoles and alkali metal ions", *Angew. Chem. Int. Ed.*, **53** (50), 13729 (Dec. 2014). [(§) equally contributing authors]

[Oral presentation at an international symposium]

1. E. Minamitani, Y. Fu, Q.-K. Xue, Y. Kim, and S. Watanabe, "Underscreened Kondo effect of the collective spin state in Mn-phthalocyanine on Pb(111)", ISSS-7 (The 7th International Symposium on Surface Science), Matsue, Japan (Nov. 2014).

2. T. K. Shimizu, J. Jung, H. Imada, and Y. Kim, "Supramolecular assembly of diarylethene via ion-dipole interaction", ISSS-7 (The 7th International Symposium on Surface Science), Matsue, Japan (Nov. 2014).

3. K. Ueji, J. Jung, J. Oh, K. Miyamura, and Y. Kim, "Thermally activated transition from 1D to 2D superstructure: squaric acid on Au(111)", ISSS-7 (The 7th International Symposium on Surface Science), Matsue, Japan (Nov. 2014).

4. H.-J. Shin, J. Jung, M. Kawai, and Y. Kim, "Dynamic process of a single molecule on an ultrathin insulating film surface by vibrational excitation with tunneling electrons", ISSS-7 (The 7th International Symposium on Surface Science), Matsue, Japan, (Nov. 2014).

5. H. Imada, M. Imai, K. Miwa, T. K. Shimizu, M. Kawai, and Y. Kim, Single-molecule luminescence spectroscopy of phthalocyanine using STM, ISSS-7 (The 7th International Symposium on Surface Science), Matsue, Japan (Nov. 2014).

6. E. Kazuma, M. Han, J. Jung, J. Oh, T. Seki, and Y. Kim, Isomerization mechanism for a single azobenzene derivative, WDPS-16 (The 16th Workshop on Dynamical Phenomena at Surfaces), Madrid, Spain (Oct. 2014).

7. H. Imada, K. Miwa, M. Imai, J. Jung, H.-J. Shin, T. K. Shimizu, M. Kawai, and Y. Kim, Single molecule chemistry and spectroscopy on ultrathin insulating films using STM, ECOSS-30 (The 30th European Conference on Surface Science), Antalya, Turkey (Aug.-Sep. 2014).

8. J. Jung, H. Lim, J. Oh, and Y. Kim, Functionalization of graphene grown on metal substrate using atomic oxygen: graphene enolate, ECOSS-30 (The 30th European Conference on Surface Science), Antalya, Turkey (Aug.-Sep. 2014).

9. H. Imada, M. Imai, T. K. Shimizu, M. Kawai, and Y. Kim, Optical processes in isolated phthalocyanines probed by scanning tunneling luminescence spectroscopy, NSS-8 (The 8th International Workshop on Nanoscale Spectroscopy and Nanotechnology), Chicago, IL, USA (Jul. 2014).

10. M. Imai, H. Imada, T. K. Shimizu, M. Kawai, and Y. Kim, "Thickness dependence of electronic structures of single H_2Pc on NaCl ultrathin insulating films", NSS-8 (The 8th International Workshop on Nanoscale Spectroscopy and Nanotechnology), Chicago, IL, USA (Jul. 2014).

11. Y. Kim, "Energetics of single-molecule chemistry", Korea-Japan Nano Forum, NANO Korea 2014 Symposium, Seoul, Korea (Jul. 2014).

12. E. Minamitani, " Kondo effects in single molecules on metal surfaces" Spintronics and Magnetochemistry on the Atomic and Molecular Level, Ascona, Switzerland

13. E. Minamitani, "DFT+NRG studies on novel Kondo effects in single molecules on metal surfaces" The 17th Asian Workshop on First-Principles Electronic Structure Calculations, Seoul, Korea